Latin American Journal of Solids and Structures
www.lajss.org

Investigation on the Effects of Process Parameters on Laser Percussion Drilling Using Finite Element Methodology; Statistical Modelling and Optimization

Abstract

In the present research, the simulation of the Nickel-base superalloy Inconel 718 fiber-laser drilling process with the thickness of 1mm is investigated through the Finite Element Method. In order to specify the appropriate Gaussian distribution of laser beam, the results of an experimental research on glass laser drilling were simulated using three types of Gaussian distribution. The DFLUX subroutine was used to implement the laser heat sources of the models using the Fortran language. After the appropriate Gaussian distribution was chosen, the model was validated with the experimental results of the Nickel-base superalloy Inconel 718 laser drilling process. The negligible error percentage among the experimental and simulation results demonstrates the high accuracy of this model. The experiments were performed based on the Response Surface Methodology (RSM) as a statistical design of experiment (DOE) approach to investigate the influence of process parameters on the responses, obtaining the mathematical regressions and predicting the new results. Four parameters i.e. laser pulse frequency (150 to 550 Hz), laser power (200 to 500 watts), laser focal plane position (-0.5 to +0.5 mm) and the duty cycle (30 to 70%) were considered to be the input variables in 5 levels and four external parameters i.e. the hole's entrance and exit diameters, hole taper angle and the weight of mass removed from the hole, were observed to be the process output responses of this central composite design. By performing the statistical analysis, the input and output parameters were found to have a direct relation with each other. By an increase in each of the input variables, the entrance and exit hole diameters, the hole taper angel, and the weight of mass removed from the hole increase. Finally, the results of the conducted simulations and statistical analyses having been used, the laser drilling process was optimized by means of the desire ability approach. Good agreement between the simulated and the optimization results revealed that the model would be appropriate for laser drilling process numerical simulation.

Keywords

Laser Drilling, Simulation, Finite Element Method, Response Surface Method (RSM)

Mahmoud Moradi [a,b,*]
Ehsan Golchin [a,b]

[a] Department of Mechanical Engineering, Faculty of Engineering, Malayer University, Malayer, Iran.
[b] Laser Materials Processing Research Center, Malayer University, Malayer, Iran.
* moradi.malayeru@gmail.com

http://dx.doi.org/10.1590/1679-78253247

Received 26.07.2016
Accepted 02.01.2017
Available online 09.01.2017

1 INTRODUCTION

One of the basic industry requirements is creating the holes in micron dimensions. So, the laser is taken to be a very useful tool for this object. The use of lasers in machining is getting extensive acceptance, especially in the sheet metal industry due to its low processing cost and high precision conferred by laser. Laser drilling is one of the significant laser machining methods, with an extensive range of applications and several types of processing objects. Laser drilling relies on melting and evaporating the material. The focused laser beam heats the material to the melting point. The arising melt is removed by a gas jet. Furthermore, the laser beam can heat the material to the evaporation point and the resulting material vapor escapes out of the hole. At this time, steam is formed and released; the waste comes out of the cavity and the molten walls around the cavity are formed (Parandoush et al., 2014, Jay Tu et al., 2014, Dubey et al., 2008)

Ghoreishi and Nakhjavani (Ghoreishi et al., 2008) studied an ANN-based process model to find the relation between process parameters (pulse frequency, power, pulse width, number of pulses, assist gas pressure, and focal plane position (FPP)) and output parameters (hole entrance and exit diameters, circularity of hole entrance and hole exit, hole taper) of laser beam percussion drilling (LBPD) using the experimental results. Pulsed Nd:YAG laser source was used to drill the 304 steel sheets with the thickness of 2.5 mm. Ganguly et al.(Ganguly et al. 2012) optimized the laser micro-drilling parameters (power, pulse frequency pulse width and air pressure) for the concurrent optimization of multi quality parameters (hole taper and width of HAZ) through the laser micro-drilling of 1mm thick zirconium oxide ceramic by grey relation analysis. Biswas et al. used an ANN-based model of laser drilling of 0.496 mm thick titanium nitride-alumina (TiN–Al2O3) composite to investigate the effect of input variables (pulse frequency, lamp current , pulse width, assist gas pressure and focal length) on output parameters (circularity at entrance hole and exit hole, hole taper). Mathematical model for laser drilling process, which calculated the effect of laser absorption by the metal vapor in the keyhole, was investigated by Solana et al. (Solana et al., 1998). They used this model to simulate the hole, and the data were in good agreement with experimental results. A 2D axisymmetric FEM model was used to analyze the process of melting and resolidification through laser drilling, using Volume of Fluid (VOF) method to track the surface of workpiece by Ganesh et al. (Ganesh et al., 1997, Ram et al., 1994). The effects of the laser power on the hole entrance diameter of the 10.0 mm thick alumina ceramic was surveyed using pulsed Nd:YAG laser in the study of Kacar et al.(Kacar et al., 2009). The hole entrance diameter and laser power were detected to have a direct relation. Hanon et al. (Hanon et al., 2012) compared the experimental and simulation data of laser drillings of 5 and 10.5 mm thick alumina ceramics using a Nd:YAG laser of 600 W. They found that peak power and duty cycle can be used effectively to change the crater depth without formation of any defects. Yinzhou et al. (Yinzhou et al., 2012) used a 2D axisymmetric FEM thermal model to predict the spatter statement and HAZ during LBPD of 4.4mm thick alumina ceramics using a CO_2 laser. It was derived that spatter deposition chiefly depends on the power and duty cycle of the laser.

In this research, at the first step, an appropriate Gaussian distribution to simulate the laser drilling process was chosen. In this phase, the parameters i.e. the depth of the holes and the speed of laser drilling were selected as the process responses. In order to validate the chosen thermal model, the results of the experimental process of Ni-base superalloy Inconel 718 fiber laser drilling and

simulation were compared through the Finite Element Method. In order to survey the influence of the input laser process parameters- laser power, laser pulse frequency, the duty cycle, and the laser focal plane position on four output responses, the entrance and exit hole diameter, the hole taper angle, and the weight of mass removed from the hole, experiments were designed through the RSM method, and the statistical analysis was performed through the Minitab 17 software. In the last step of research, with the process optimized through the desire ability approach, the optimal parameters of the process were obtained and compared with the simulated result.

2 FINITE ELEMENTS SIMULATION

2.1 Governing Equations and the Boundary Conditions

In laser drilling process, there are plenty of complexities such as the immediate change of phase, high temperature gradient and the plasma producing. To simulate this process, the model being used is required to transform into a more simple form in comparison to the real form of the process. In order to perform the simulations, the following hypotheses have been taken into consideration:

1. The model is considered in a homogenous form.
2. The plasma creation and multiple reflections inside the hole were ignored.
3. Shockwave production was negligible.
4. Energy absorption through molten material was ignored.
5. The heat transfer within the melt pool was ignored
6. The material properties were considered as the temperature-dependent.

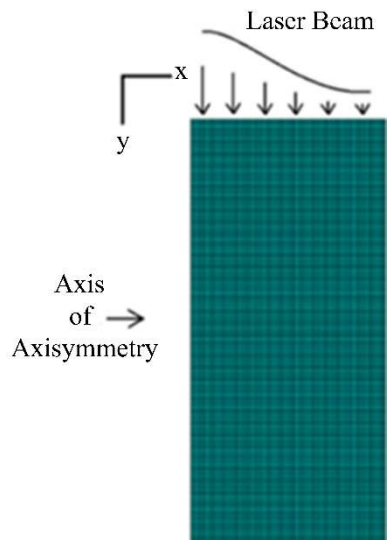


Figure 1: Finite Element Model for laser drilling (Yinzhou et al., 2012).

The overall analysis form of laser drilling process through Finite Element Method is shown in Figure 1. The analyses conducted in this research have merely been the thermal analyses, aimed to obtain the element temperature in different nodes and times. The temperature in different points depends on input heat and the material thermal properties. According to the Fourier's law, the

temperature of each point of the material is obtained through Equation 1. Equation 1 expresses the Fourier's heat transfer within a cylindrical form (Mishra et al., 2013):

$$k(T)\left[\frac{1}{r}\frac{\partial}{\partial r}\left(\frac{\partial T(r,z,t)}{\partial r}\right)+\frac{\partial^2(r,z,t)}{\partial z^2}\right]=\rho(T)\,C(T)\frac{\partial T(r,z,t)}{\partial t} \tag{1}$$

where ρ(T) is the temperature-dependent density; C(T) is the temperature-dependent special heat and the K(T) is the temperature-dependent heat transfer coefficient. The mentioned properties for the homogenous materials are constant in all direction, and the used materials in this research are homogenous.

The initial temperature of the model is assumed to be equal to the ambient temperature, T0. So, T(r, z, 0) =T_0. On the t=0, the input energy to the material is equal to the input temperature. According to Equation (1) and by applying the initial conditions, the governing thermal boundary conditions of the mode are presented in equations 2-4. In Equations (2) to (4), τ is the pulse-on-time and tp is the total pulse time (Mishra et al., 2013).

When $0 < t < \tau$*:*

$$k(T)\frac{\partial(r,z,t)}{\partial z}=\begin{cases}h(T(r,z,t)-T_0) & for\ r>R\ on\ B_1\\ q_{in} & for\ r\le R\ on\ B_1\end{cases} \tag{2}$$

Whenever $\tau < t < tp$*:*

$$k(T)\frac{\partial(r,z,t)}{\partial z}=h(T(r,z,t)-T_0)\ on\ B_1 \tag{3}$$

Whenever $t > 0$*:*

$$k(T)\frac{\partial(r,z,t)}{\partial n}=0\ on\ B_2, B_3\ and\ B_4 \tag{4}$$

Each material at a temperature higher than its ambient temperature radiates energy. In the laser drilling, the material surface temperature faces severe changes. Therefore, radiation is considered to be a highly significant factor in this process. The heat flux radiated from substance's surface is expressed by the Stefan-Boltzmann law (Akarapu et al., 2004):

$$q_rad=\sigma\in(Ts\hat{}4-T\infty\hat{}4) \tag{5}$$

where σ is the constant value of the Boltzmann equal to 5.67×10-8 , and ∈ is the radiation coefficient equal to 0.9. Furthermore, T_s and T_∞ are the material surface temperature and the ambient temperature, respectively. On the conducted simulations, the ambient temperature is given as 298 ° K.

To consider the losses of the heat as the result of the cooling jet-gas, the convective conductivity was assumed to be 200W/(m^2 k) . The convection heat flux by the Newton Cooling Law is expressed as Equation 6 (Akarapu et al., 2004).

$$q=Ah(T_s-T_\infty) \tag{6}$$

In equation (6), A is the area of the object, h is the heat transfer coefficient, T_s is the material surface temperature and T_∞ is the ambient temperature which is given as 298 ° K.

2.2 Simulation Method

Due to the circularity of the hole sections and also the laser beam, the process modeling can be performed in an axisymmetric form. The most outstanding benefit of axisymmetric modeling is the reduction of the number of elements and, consequently, the reduction of the problem-solving time. Figure 2 illuminates the ideal case in which a laser beam has been modeled as a heat source with Gaussian-distributed heat flux with suitable boundary conditions considering the axisymmetric model of the analysis.

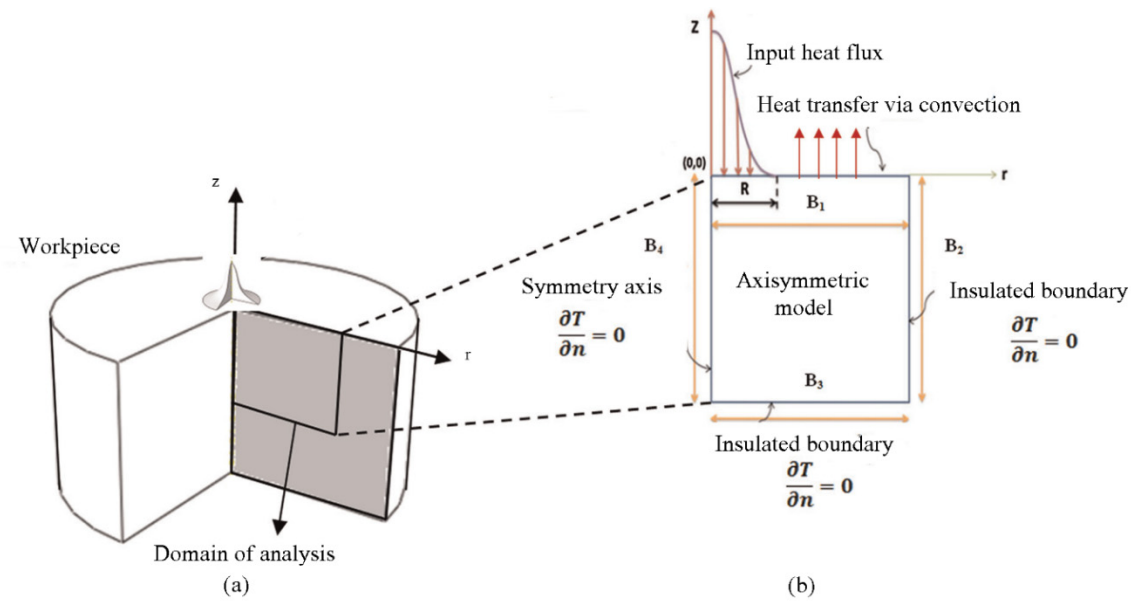


Figure 2: Thermal model of laser drilling process a) Schematic representation of the workpiece. b) Axisymmetric model with boundary condition.

The simulations in this research have been performed through the ABAQUS software. The heat flux load was programmed in FORTRAN as DFLUX subroutine. In order to remove those elements the temperature of which has exceeded the evaporation point, the element death technique has been used.

2.3 Selecting an Appropriate Heat Source Model

Gaussian distribution is one of the closest distributions for the laser heat flux. To select the most appropriate Gaussian distribution for the laser heat flux in laser drilling process, the results of the experimental glass laser drilling process (Yi Zhang et al., 2013) were compared with those obtained from three types of simulations with different distributions. Table 1 shows the specifications of the used laser for glass laser drilling.

Parameter	Type / Amount
Laser type	CO_2
Type of wave	Continuous
Power	1325 W
Beam Diameter at the Lens	30 mm
Beam Diameter at Focal Point	0.5 mm
Focal length	178 mm
wave length	1060 nm
M^2	1.05
Assist Gas	Argon

Table 1: Laser Parameters used for glass drilling.

In the first type of simulation, the distribution presented in Equation 7 has been used (Yi Zhang et al., 2013).

$$I(r,z) = \frac{2AP}{\pi\omega(z)^2} exp\left(-2\frac{r^2}{\omega(z)^2}\right)$$
$$\omega(z) = \omega_0\sqrt{1+(\frac{z\omega_m}{f\omega_0})^2} \tag{7}$$

In Equation 7, P is the laser power, A is the absorption coefficient, ωm is the radius of the laser beam in the focal plane position, ω0 is the radius of the focal point, r is the radial distance from the laser axis, z is the perpendicular distance from the laser focal point, and f is the laser focal distance. Equation 8 has been used for the second type of simulation (Mishra et al., 2013):

$$Q_{in} = \frac{2AP}{\pi R^2} exp\left(-2\frac{r^2}{R^2}\right)$$
$$R = \frac{d}{2}\left[1+\left(4\ \frac{M^2\ L\ (z+f)}{\pi d^2}\right)\right] \tag{8}$$

In Equation 8, A is the absorption coefficient, P is the laser power, R is the laser effective radius, r is the laser beam radius, L is the laser wavelength, d is the laser beam diameter and f is the laser focal distance.

In simulation type 3, Equation 9 has been used (Yiming Zhang et al., 2014):

$$q(r) = \eta Q/(\pi r_q\hat{}2)exp(-r\hat{}2/(r_q\hat{}2)) \tag{9}$$

In Equation 9, the value of η is the material absorption coefficient, Q is the laser power, r_q is the laser beam radius, and r is radial distance from the laser beam axis.

The 8-node hexahedral elements, DCAX4, were used for the transient thermal analysis. 5 micrometers was chosen as the element optimal length by mesh sensitivity which has been carried out through the trial and error method.

The three types of simulation and experimental results of the glass drilling are presented in Table 2. Figures 3 and 4 illustrate depth of holes and drilling velocity of simulated and experimental results, respectively.

As Table 2, Figures 3 and 4 show, in comparison of the experimental results and the glass laser drilling simulations, the Gaussian distribution No.2, Equation 8, has the best agreement with the experimental results. Therefore, Equation 8 can be used in simulating the drilling process in the next stages.

No	Drilling Time	Experimental results		Simulation1		Simulation 2		Simulation 3	
		Depth (mm)	Velocity (mm/ms)	Depth (mm)	Velocity (mm/ms)	Depth (mm)	Velocity (mm/ms)	Depth (mm)	Velocity (mm/ms)
1	5	1.624	0.324	1.505	0.301	1.635	0.327	1.200	0.240
2	10	3.05	0.305	3.000	0.300	3.255	0.325	3.000	0.300
3	15	4.23	0.282	4.250	0.283	4.445	0.296	3.895	0.265
4	20	5.18	0.259	5.305	0.265	5.000	0.250	4.685	0.234
5	25	5.90	0.236	5.885	0.235	6.005	0.240	5.560	0.222
6	30	6.35	0.211	6.365	0.232	6.155	0.205	6.155	0.205
7	35	7.10	0.202	7.115	0.203	7.000	0.200	6.735	0.192
8	40	7.65	0.191	7.650	0.191	7.775	0.194	7.285	0.182
9	45	8.20	0.182	8.215	0.182	8.275	0.183	7.900	0.175
10	50	8.56	0.171	8.535	0.171	8.600	0.172	8.120	0.162
11	55	8.92	0.162	8.945	0.162	9.005	0.163	8.560	0.155
12	60	9.55	0.159	9.625	0.160	9.490	0.158	9.215	0.153

Table 2: Experimental and Simulated results of glass laser drilling.

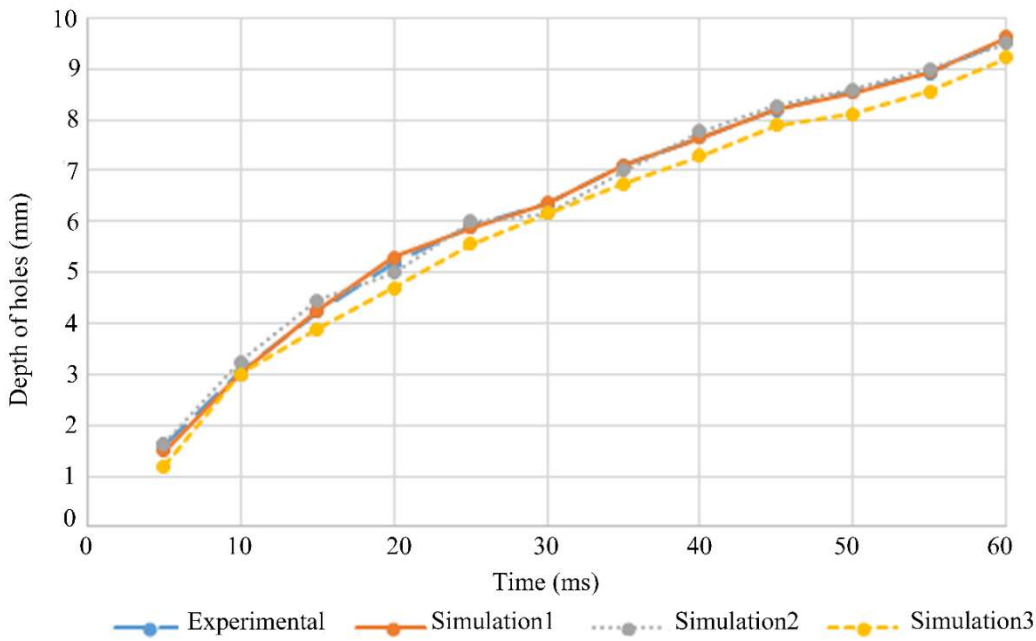


Figure 3: Comparison between depth of holes in experimental and simulated glass laser drilling.

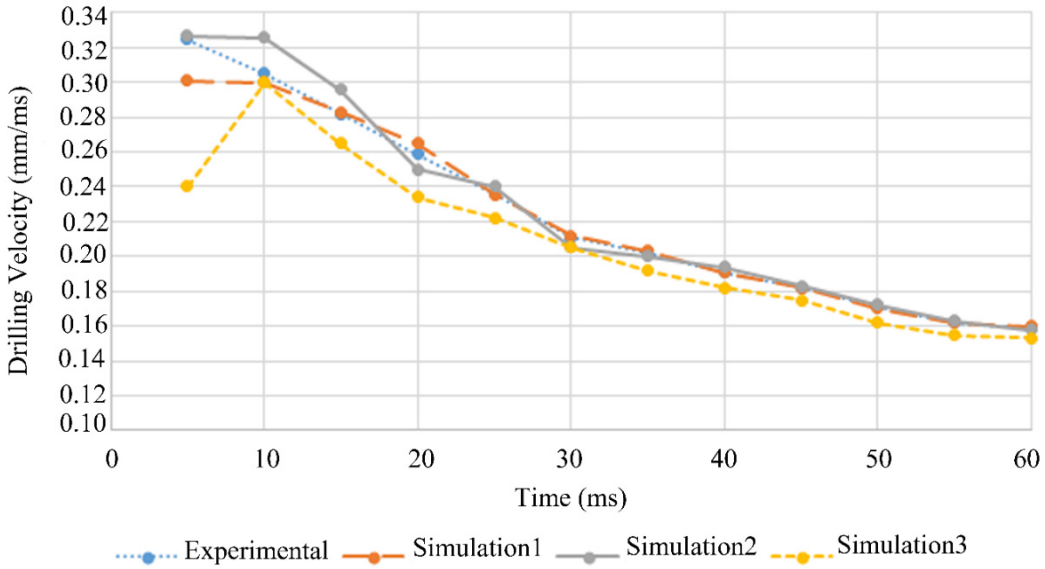


Figure 4: Comparison between drilling velocity in experimental and simulated glass laser drilling.

3 EXPERIMENTAL PROCESS AND MODEL VERIFICATION

In order to verify the suggested model, Equation 8 presented in section 2.3, three laser drilling experimental tests were performed on the Nickel-base superalloy Inconel 718 with the thickness of one millimeter. The thermo-physical material properties incorporated in the experimental research are presented in Table 3. Fiber laser with the 80- micrometer beam focus diameter was utilized in the experiments.

In the experiments, duty cycle was 50% and the laser focal plane position was equal to 1mm above the workpiece. The overall drilling time in all the three experiments was 0.1 seconds. Figure 5 depicts the experimental process. The experimental conditions are shown in Table 4.

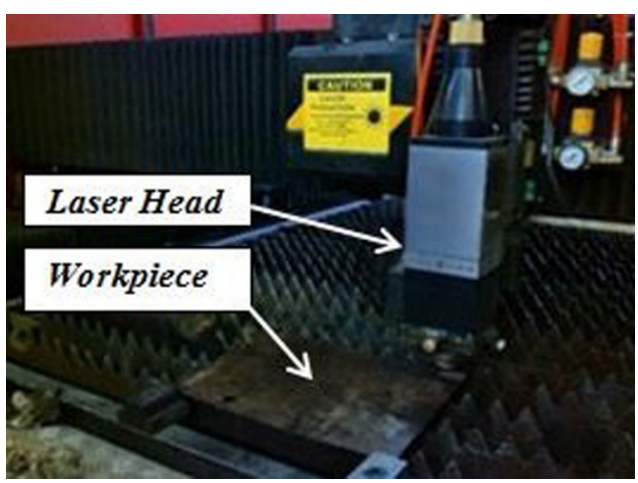


Figure 5: Experimental set-up of laser drilling.

Temperature (K)	Density ($Kg.m^{-3}$)	specific heat ($J.Kg^{-1}.K^{-1}$)	Thermal conductivity ($W.m^{-1}.K^{-1}$)
298	8240	439	10.3
373	8221	454	11.5
473	8293	473	13.2
573	8162	493	15
673	8130	512	16.9
773	8095	532	18.8
873	8058	551	20.9
973	8019	582	22.8
1073	7978	604	23.8
1173	7934	626	25.9
1273	7889	648	28
1373	7841	670	30.2
1473	7792	692	32.4
1573	7761	710	33.7
1628	7420	677	29
1673	7363	677	29
1773	7280	677	29

Table 3: Thermo-physical properties of Inconel 718 used in simulations (Mills 2002).

The geometry features of the entrance and exit hole diameters were measured using Axioskop 40 optical microscope at a magnification of 1000× and the images were exactly measured by the Visilog software. According to Figure 6 and Equation 10, by using the entrance and exit diameters, the value of the taper angle can be achieved.

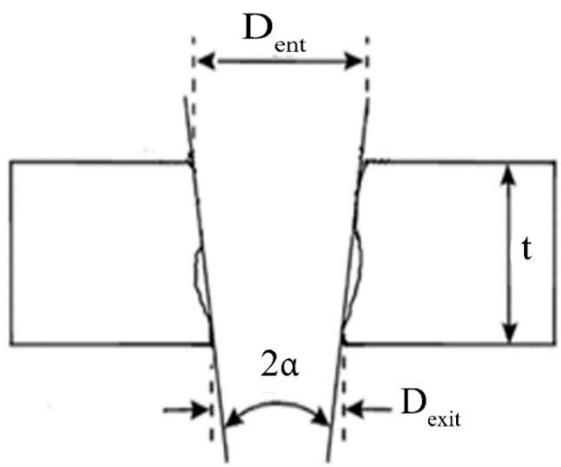


Figure 6: The Geometry of hole.

$$Taper(°) = \frac{d_{entrance} - d_{exit}}{2t} \times \frac{180}{\pi} \tag{10}$$

Where the ($d_{entrance}$) is entrance hole diameter, (d_{exit}) is exit hole diameter, and t is the thickness of the material.

Simulation procedure in this step is the same as the one presented in Section 2-3. Table 4 shows the different values of hole geometry obtained according to the laser drilling parameters set for the verification experiments along with the amounts of relative verification errors using the simulated approaches.

No	Setting			Entrance Diameter			Exit Diameter			Hole Taper Angle		
	Laser Power (w)	Laser Pulse Frequency (Hz)	Focal Plane Position (mm)	Experimental	Simulation	Error (%)	Experimental	Simulation	Error (%)	Experimental	Simulation	Error (%)
1	404	248	1	404	480	-9.09	304	310	-1.97	3.9	4.86	-24.61
2	423	200	1	449	420	6.9	317	300	5.36	3.8	3.43	9.73
3	383	274	1	480	460	4.16	330	320	3.03	3.4	4	-17.64

Table 4: Comparison between simulation and experimental results of Inconel 718.

Low error values yielded by the present model, illustrated in Table4, can guarantee the suitability and logics of the modeling assumptions in this study. Inaccuracy in measuring the entrance and exit diameters in experimental tests, difference between the theoretical and real values of the experimental input parameters such as laser beam radius, laser absorption coefficient and material temperature-dependent properties could be the reasons of variation between the software and experimental results.

Figure 7 depicts the final shape and temperature distribution of the hole after the simulation process is conducted and element death is performed, while Figure 8 illustrates a comparative image between the experimental and the simulation.

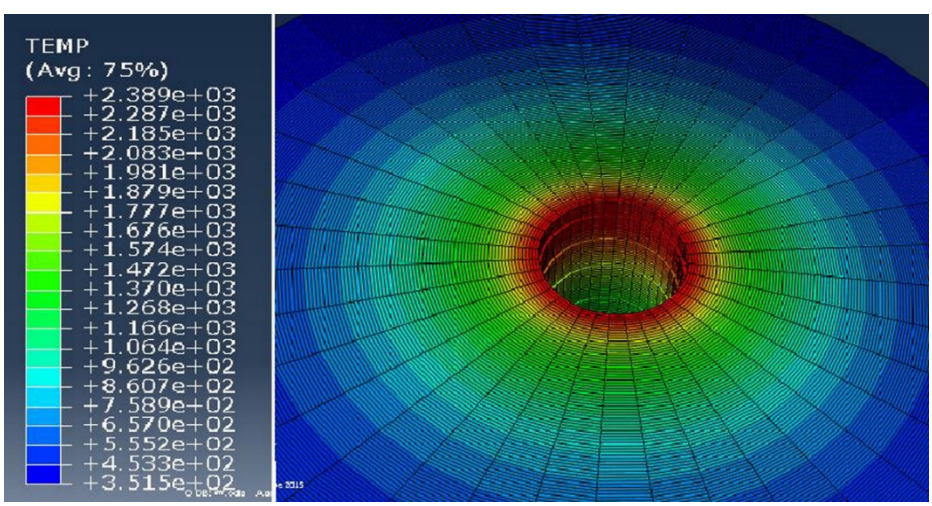


Figure 7: Temperature distribution of Inconel 718 laser drilling

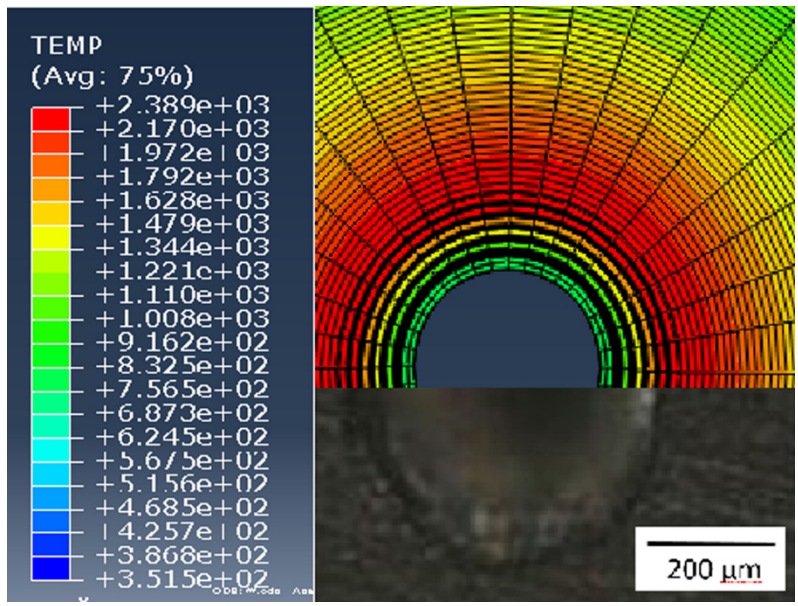


Figure 8: Comparison between simulated and experimental results (Temperature unit is centigrade).

4 EXPERIMENTAL DESIGN AND METHODOLOGY

Response Surface Methodology (RSM) is a set of statistical techniques and applied mathematics to investigate responses (output variables) affected by a number of independent variables (input variables). In each experiment, changes in input variables are made to determine the cause of changes in the response variable (Montgomery 2009). The purpose is to find a relationship between outputs and inputs (responses and parameters) with a minimum error in the form of a mathematical model. Depending on the type of input variable parameters, there are, in general, different ways to design an experiment.

The Response Surface Methodology, RSM, is considered to be a set of mathematical and statistical techniques useful for modeling and predicting the desired response (Mahmoud Moradi et al., 2011, Mahmoud Moradi et al., 2014). Also, the RSM specifies the relationships between one or more measured responses and the essential controllable input factors (Mahmoud Moradi et al., 2014).

In the present study, Response Surface Methodology is chosen as the method of design. When all the independent variables are capable of being measured and controlled during an experiment, the response surface is to be expressed as a function through Equation 11.

$$Y= f(x1, x2, x3,....., xk) \tag{11}$$

Here, "k" is the number of independent variables. It seems essential to find a rational function to relate the independent variables to the responses. Therefore, a quadratic polynomial function presented in Equation 12 is usually applied in response surface methodology.

$$y = \beta_0 + \sum_{i=1}^{k} \beta_i x_i + \sum_{i=1}^{k} \beta_{ii} x_i^2 + \sum_{i} \sum_{j} \beta_i x_i x_j + \varepsilon \tag{12}$$

In the above equation, β is constant, βi is linear coefficient, βii is coefficient of quadratic, βij is interaction coefficient and ε is the error of the parameters of regression (Mahmoud Moradi et al., 2013). In the present study, after model validation, laser pulse frequency, the duty cycle, the laser power and laser focal plane position were considered to be independent input parameters. Table 5 shows four input variables of the experiment, coded values and actual values of their surfaces. The focal plane position, FPP, was considered as zero when set on upper material surface. Above or below the upper surface, the FPP was considered as positive or negative, respectively. Schematic diagram of FPP is illustrated in Figure 9.

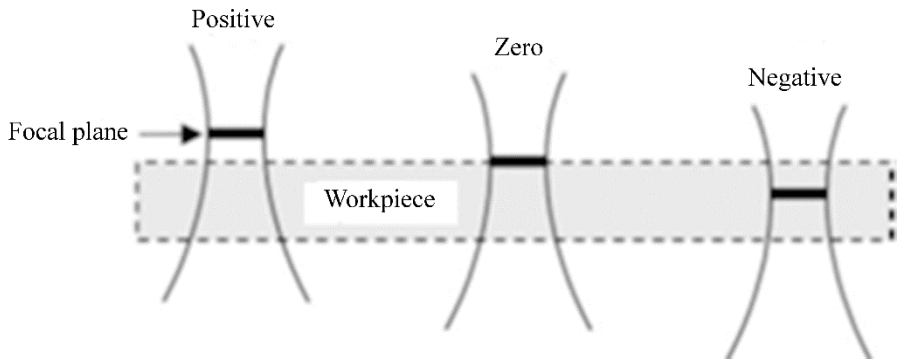


Figure 9: Variation of focal Plane position on the work piece (Ghoreishi et al., 2002).

In the present study, in order to perform the simulation tests, central composite design (CCD), five-level RSM design with four parameters, presented in Table 6, was applied. This plan includes sixteen experiments as factorial points in cubic vertex, eight experiments as axial points and one experiment in the cubic center as center point experiment, meaning a total of 25 experiments have been designed.

The designed experiments have been performed on the Nickel-base superalloy Inconel 718with the thickness of 1mm. Initial temperature of 298 ° K, the convection coefficient of 20W/(m^2 k) and the radiation coefficient equal to 0.9 were considered as the thermal boundary conditions. The interaction time of laser with material is taken to be 0.1 s. The design matrix of the experiments and the obtained results are shown in Table 5.

Variable	Sign	Unit	-2	-1	0	+1	+2
Laser Pulse Frequency	F	(Hz)	150	250	350	450	550
Laser Power	P	(W)	200	275	350	425	500
Focal Plane Position	FPP	(mm)	-0.5	-0.25	0	+0.25	+0.5
Duty cycle	D	(%)	30	40	50	60	70

Table 5: Independent process parameters with design levels.

No	Input Setting				Responses			
	Laser Pulse Frequency	Laser Power	Focal plane Position	Duty cycle	Entrance hole diameter (μm)	Exit hole diameter (μm)	Taper angle	Weight of removed mass (mg $\times 10^{-5}$)
1	0	0	0	2	480	230	7.16	84.93
2	2	0	0	0	490	220	7.73	85.22
3	0	0	0	0	400	170	6.58	55.42
4	1	-1	1	-1	410	160	7.16	55.94
5	0	2	0	0	540	260	7.99	107.78
6	1	-1	-1	1	400	150	7.16	52.31
7	1	-1	1	1	440	170	7.73	64.13
8	-1	1	-1	-1	460	200	7.44	74.12
9	-1	-1	-1	1	390	140	6.58	48.82
10	1	1	-1	-1	380	210	4.86	80.96
11	-1	-1	1	1	420	160	7.44	58.07
12	0	0	-2	0	340	120	6.30	36.84
13	-1	1	1	-1	480	200	8.01	79.04
14	-1	1	1	1	490	200	8.30	81.56
15	1	-1	-1	-1	390	150	6.87	50.28
16	-1	-1	1	-1	390	160	6.58	54.87
17	1	1	1	-1	490	210	8.01	83.51
18	-2	0	0	0	320	110	6.01	32.29
19	0	0	2	0	460	200	7.44	74.12
20	-1	-1	-1	1	470	200	7.23	76.56
21	0	0	0	-2	310	90	6.30	28.50
22	1	1	1	1	620	330	8.30	150.55
23	-1	-1	-1	-1	300	120	5.15	30.29
24	1	1	-1	1	500	220	8.01	88.10
25	0	-2	0	0	250	100	4.29	21.03

Table 6: Design Matrix and experimental results.

5 RESULTS AND DISCUSSION

The results of measuring the entrance and exit hole diameters, hole taper and weight of removed material were considered as the responses of the experiment. Analysis of variance (ANOVA) was employed in order to investigate significant effective parameters on laser drilling simulation process and to interpret the effect of the results by using Minitab17 statistical software. The results show that by controlling the input process parameters, the proper responses could be achieved. In this analysis, full quadratic polynomial function was used.

5.1 Entrance Hole Diameter:

In the analysis of variance tables, the P-value expresses the response sensitivity to the input parameters, and by a decrease in P-value the sensitivity increases. So, in the concept of statistical modeling, the lower the P-value, the more influential the effect. When the P-value in the analyses of variances is less than 0.05, the term is distinguished as significant (Ghoreishi et al., 2002).

According to the results of analysis of variance on the entrance hole diameter, Table 7, all the main effects of four input parameters; laser power (P), laser pulse frequency (F), duty cycle (D), and the laser focal plane position (FPP) have respectively the highest influences on the diameter of the entrance hole, and all were identified as the effective linear terms. But none of the quadratic and interaction terms were identified as the significant terms. The regression equation obtained is evaluated as significant and Lack-of-Fit as insignificant. In the best analysis, regression is significant and Lack-of-Fit insignificant. Therefore, according to the analysis, the final regression in terms of coded parameter values yields in Equation (13).

$$D_{in} = 428.80 + 27.92\ F + 59.58\ P + 24.58\ FPP + 27.92\ D \tag{13}$$

An increase in the laser pulse frequency, the laser power and the duty cycle causes an increase in the amount of the thermal flux absorbed by the material and, as a result, it causes an increase in entrance hole diameter. Figures 10 and 11 illustrate response surfaces of entrance hole diameter in terms of input parameters.

Source	Degree of freedom	Adj Sum of squares	Adj Mean squares	T- Value	F-Value	P-Value
Model	4	137117	34297	----	23.85	0.000
Linear	4	137117	34297	----	23.85	0.000
Laser pule Frequency	1	18704	18704	3.61	13.01	0.002
Laser Power	1	85204	85204	7.70	59.28	0.000
Focal Plane position	1	14504	14504	3.18	10.09	0.005
duty cycle	1	18704	18704	3.61	13.01	0.002
Error	20	28747	1437			
Total	24	165864				
R-sq = 82.67 %		R-sq (adj) = 79.20 %				

Table 7: Revised analysis of variance of entrance hole diameter.

As shown in Figure 10, by an increase in laser pulse frequency and laser power, entrance hole diameter increases. These two parameters (laser pulse frequency and laser power) having increased simultaneously, the pulses applied to the material surface will impact the workpiece with shorter interval and higher energy, which results in receiving more heat by the surface and as a result the substance melts down more thus entrance hole diameter increases.

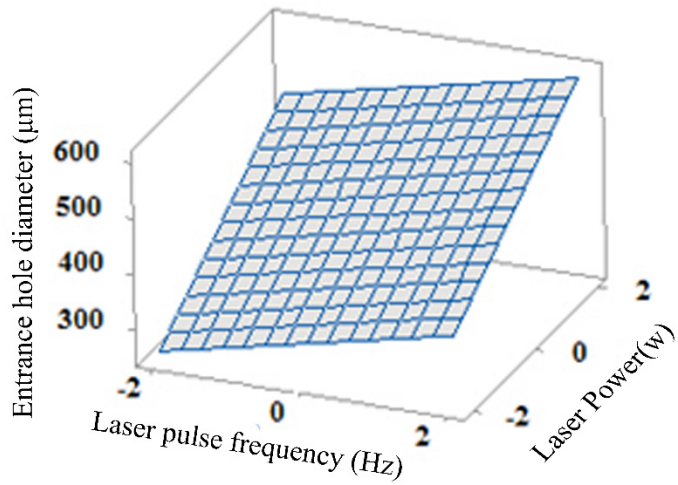


Figure 10: The entrance hole diameter response surface in terms of laser power (P) and laser pulse frequency (F).

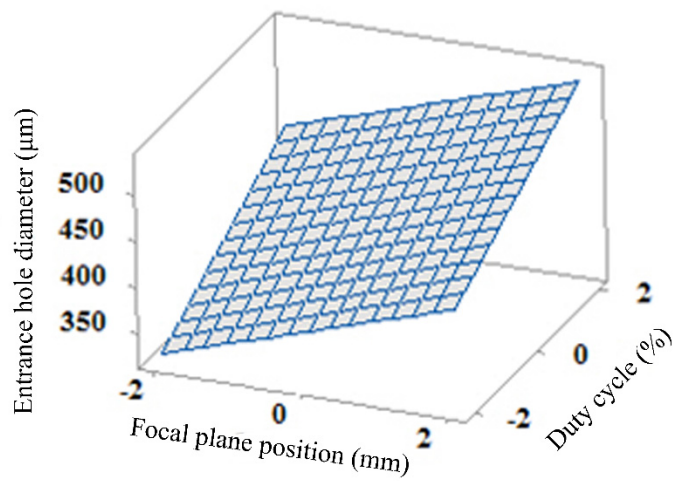


Figure 11: The entrance hole diameter response surface in terms of duty cycle (D) and focal plane position (FPP).

As it is obvious in Figure 11, an increase in the laser duty cycle (D), and the laser focal plane position (FPP) causes an increase in diameter of the entrance hole. Due to the higher duty cycle, pulse energy increases per pulse, and increase in the average laser power increases the accumulation of heat input on the workpiece. And, also with an increase in the laser focal plane position, the focal point is formed at the top surface of the workpiece and the diameter of the applied laser beam at the interaction point with the workpiece surface increases, see Figure 9. Consequently, this will cause an increase in the area affected by the laser heat and subsequently the entrance hole diameter increases.

5.2 Exit Hole Diameter:

Table 8 shows analysis of variance for the diameter of the exit hole. As shown in Table 8, all main parameters are considered as significant terms and none of the other interaction and quadratic terms are significant. As Table 8 indicates, Lack-of-Fit was determined as insignificant and it shows that a suitable analysis has been performed. Considering the P-Value, laser power, laser pulse frequency, laser duty cycle and the laser focal plane position have the highest influence on the exit hole diameter.

According to the performed analysis in ANOVA Table 8, equation 14 represents the regression equation for the exit hole diameter considering significant parameters based on coded values. In the equation (14), which is a linear equation, it should be mentioned that all the main parameters have a positive effect on this response.

$$D_{out} = 428.80 + 27.92\ F + 59.58\ P + 24.58\ FPP + 27.92\ D \quad (14)$$

Source	Degree of freedom	Adj Sum of squares	Adj Mean squares	T- Value	F-Value	P-Value
Model	4	53800	13450.0	----	16.83	0.000
Linear	4	53800	13450.0	----	16.83	0.000
Laser pule Frequency	1	8067	8066.7	3.18	10.09	0.005
Laser Power	1	32267	32266.7	6.35	40.37	0.000
Focal Plane position	1	5400	5400.0	2.60	6.67	0.017
duty cycle	1	8067	8066.7	3.18	10.09	0.005
Error	20	15984	799.2			
Total	24	69784				
R-sq = 77.10 %		R-sq (adj) = 72.51 %				

Table 8: Revised analysis of variance of exit hole diameter.

An increase in the experiment input parameters causes the higher heat absorption at the surface of workpiece, and then the absorbed heat penetrates into the depth of the workpiece resulting in an increase in the lower workpiece surface temperature and consequently causes an increase in the exit hole diameter.

5.3 Hole Taper

Table 9 shows the variance analysis of the hole taper. The only effective parameters are laser power, laser pulse frequency and the focal plane position. Final regression equation of the hole taper response, based on the significant parameters, is shown in Equation 15 based on coded values.

$$\text{Taper}\ (^\circ) = 7.111 + 0.332F + 0.668\ P + 0.307\ FPP \quad (15)$$

Increasing the laser pulse frequency, the laser power and the laser focal plane position leads to an increase in the entrance and exit hole diameters. Taking into consideration that the increase in the diameter of the entrance hole is more than the increase in the exit hole diameter, the taper angle of the hole increases. The increase in duty cycle results in an equal increase in the entrance and exit hole diameters, therefore the hole taper angle does not change a lot by varying the duty cycle.

Consequently, the duty cycle parameter can be defined as an insignificant parameter on the hole taper angle degree, as the statistical analysis confirm it. Figure 12 illustrates the effects of the laser pulse frequency and the laser power on the hole taper angle.

Source	Degree of freedom	Adj Sum of squares	Adj Mean squares	T- Value	F-Value	P-Value
Model	3	15.617	5.2057	----	14.45	0.000
Linear	3	15.617	5.2057	----	14.45	0.000
Laser pule Frequency	1	2.640	2.6401	2.71	7.33	0.013
Laser Power	1	10.720	10.7201	5.46	29.77	0.000
Focal Plane position	1	2.257	2.2571	2.50	6.27	0.021
Error	21	7.563	0.3602			
Total	24	23.180				
R-sq = 67.37 %		R-sq (adj) = 62.71 %				

Table 9: Revised analysis of variance of hole taper angle.

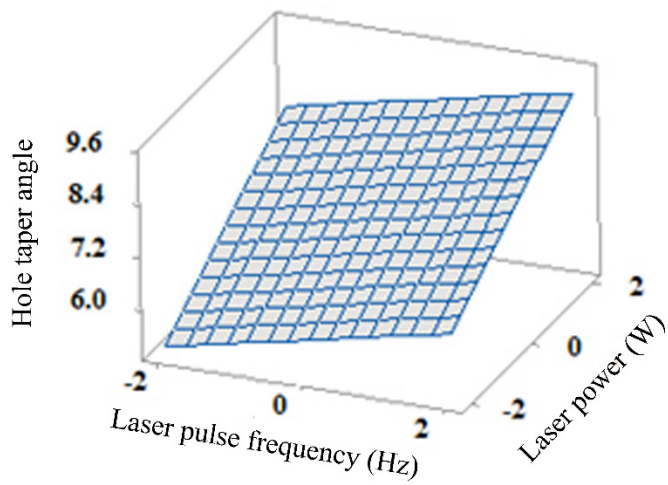


Figure 12: The hole taper angle response surface in terms of laser power (P) and laser pulse frequency (F).

As shown in Figure 12, the laser power and the laser pulse frequency having increased, the hole taper angle will increase, the reason of which is the increase in the entrance and exit hole diameters in unequal proportions.

5.4 Weight of Removed Material

Table 10 shows variance analysis of the weight of removed material. As shown in Table 10, all main parameters are considered as significant terms and none of the other interaction and quadratic terms are significant. According to the performed statistical analysis it becomes clear that the laser power, the duty cycle, the laser focal plane position and the laser pulse frequency have the highest

influences on the weight of removed material respectively. Therefore, according to the analysis, the final regression in terms of coded parameter values yields in Equation 16:

$$RM = 66.22 + 9.54\ F + 19.72\ P + 8.37\ FPP + 9.33\ D \tag{16}$$

Source	Degree of freedom	Adj Sum of squares	Adj Mean squares	T- Value	F-Value	P-Value
Model	4	15282	3820.6	----	19.86	0.000
Linear	4	15282	3820.6	----	19.86	0.000
Laser pule Frequency	1	2183	2183.3	3.37	11.35	0.008
Laser Power	1	9330	9329.5	6.96	48.49	0.000
Focal Plane position	1	1680	1679.9	3.95	8.73	0.008
duty cycle	1	2090	2089.7	3.30	10.86	0.004
Error	20	3848	192.4			
Total	24	19130				
R-sq = 77.10 %		R-sq (adj) = 72.51 %				

Table 10: Revised analysis of weight variance of removed material.

Due to an increase in the input process parameters, the amount of input heat energy absorbed by the workpiece surface increases resulting in melting down more material. Subsequently, the hole dimensions get larger and also the weight of material removed from the hole increases, too.

6 OPTIMIZATION

By statistical analysis of data obtained from simulation tests, regression equations explain logical relations between input variables and responses. The response optimizer option within the DOE module of Minitab 17 statistical software package has been used here to optimize input parametric combinations resulting in the most desirable compromise between different responses using desirability function (Saeed Assarzadeh et al., 2015). Table 11 summarizes criterions in order to optimize process parameters. Minimum hole taper and minimum entrance hole diameter are the criteria of the optimization. The reason of not considering the exit hole diameter and the weight of removed material in optimization criteria is that these two responses are dependent on the entrance hole diameter and the extent of taper angle. Whenever the entrance hole diameter and the taper angle are optimized, the exit hole diameter and the weight of removed material will be in an optimized condition, too.

In the optimization procedure presented in Table 11, the weight values of the responses are mentioned. Figure 13 shows the visual representation of the optimization result**.** The optimization plot displays the effect of each parameter (columns) on the response or composite desirability (rows). Moreover, each cell presents how the response varies as a function of one of the input process parameters while the other parameters are kept fixed. Also, the vertical lines inside the cells show current optimal parametric settings whereas the spotted horizontal lines denote the current response values. The most important part is the optimal parameter settings required to realize the process criteria, located at the middle row between the high and low row, symbolized by “cur” and

expressed in coded procedure. As it can be seen in Figure 13, all input parameters should be on -2 level, the least value of each parameter, to create an optimized hole.

No	Parameter/Response		Goal	Lower	Target	Upper	Weight	Importance
1	Parameters	Frequency	Is in range	150	---	550	---	---
2		duty cycle	Is in range	30	---	70	---	---
3		focal plane position	Is in range	-0.5	---	+0.5	---	---
4		laser power	Is in range	200	---	500	---	---
5	Responses	D (ent)	Minimum	250	250	620	3	3
6		Hole taper	Minimum	4.29	4.29	8.3	5	5

Table 11: Constraints and criteria of input parameters and responses.

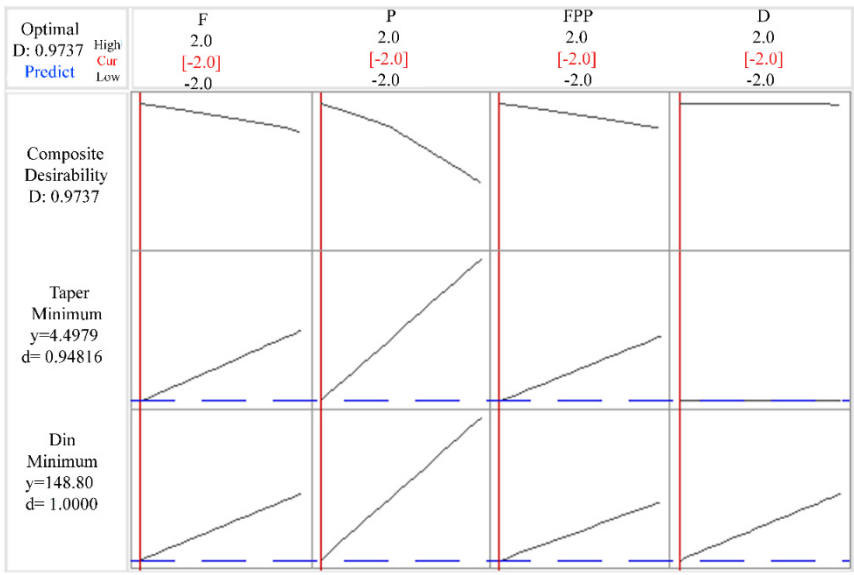


Figure 13: Calculation of optimal parameters.

Verification simulation was performed at the obtained optimal input parametric setting to compare the actual entrance and exit hole diameter and hole taper with those as optimal responses obtained from optimization. Table 12 presents the optimization results along with simulation obtained responses and their percentage relative verification errors. It is clear that the error percentage of the study is good for engineering applications.

No	Optimized Settings				Type of response	Responses	
	Laser pulse frequency (Hz)	Laser power (W)	Duty cycle (%)	Focal plane position (mm)		Entrance hole diameter (μm)	Taper angle
1	150	200	30	-0.5	Predict	148.8	4.498
					Simulation	170	3.436
					Error (%)	-14.24	23.61

Table 12: Optimum prediction results and simulation validation.

7 CONCLUSIONS

In the present study, the process of laser percussion drilling was simulated using finite element method. The data obtained from the simulated tests were analyzed through DOE. Regarding the performed simulations and statistical analyses, the following conclusions can be drawn:

1. Utilizing all the variable parameters of the laser in Gaussian distribution, such as the wavelength, M2 parameters and the laser focal plane position, is necessary.
2. By an increase in the laser power, the laser pulse frequency, the laser duty cycle and the laser focal plane position, the entrance and exit hole diameters, the hole taper angle and the extent of the weight of material removed from the hole are increased.
3. The laser duty cycle effect on the extent of the hole taper angle was insignificant statistically.
4. By performing optimization process, using desirability approach, the minimum level of each parameter can be described as the optimum setting of the laser drilling simulation process.

Acknowledgments

The authors would like to thank Malayer University for the financial support of this research.

References

Akarapu, R., Li, B.Q., Segall, A. (2004). A Thermal Stress and Failure Model for Laser Cutting and Forming Operations. journal of Failure Analysis and Prevention . 5 , 51-62.

Dubey, A.K. V. Yadava. (2008). Experimental study of Nd:YAG laser beam machining—An overview. Journal of Materials Processing Technology 195: 15-26.

Ganesh, R.K., A. Faghri, and Y. Hahn. (1997). A generalized thermal modeling for laser drilling process—II. Numerical simulation and results. International Journal of Heat and Mass Tranfer 40: 3361-3373.

Ganesh, R.K., A. Faghri, Y. Hahn. (1997). A generalized thermal modeling for laser drilling process—I. Mathematical modeling and numerical methodology. International Journal of Heat and Mass Transfer. 40, 3351-3360.

Ganguly D, A.B., Kuar. AS,Mitra S. (2012). Hole characteristics optimization in Nd:YAG laser micro-drilling of zirconium oxide by gray relational analysis. Adv Manuf Technol 61: 1255-1262.

Ghoreishi, M. O.B. Nakhjavani. (2008). Optimisation of effective factors in geometrical edifications of laser percussion drilled holes. Journal of Materials Processing Technology 196: 303-310.

Ghoreishi, M., D.K.Y. Low, L. Li. (2002). Comparative statistical analysis of hole taper and circularity in laser percussion drilling. International Journal of Machine Tools and Manufacture 42: 985-995.

Hanon M.M., E. Akman, B. Genc Oztoprak, M. Gunes, Z.A. Taha, K.I. Hajim, E. Kacar, O. Gundogdu, A. Demir. (2012). Experimental and theoretical investigation of the drilling of alumina ceramic using Nd:YAG pulsed laser. Optics and Laser Technology 44: 913-922.

Jay Tu, Alexander G. Paleocrassas, Nicholas Reeves, Nilesh Rajule. (2014). Experimental characterization of a micro-hole drilling process with short micro-second pulses by a CW single-mode fiber laser. Optics and Lasers in Engineering 55: 275-283.

Kacar E., M. Mutlu, E. Akman, A. Demir, L. Candan, T. Canel, V. Gunay, T. Sınmazcelika. (2009). Characterization of the drilling alumina ceramic using Nd:YAG pulsed laser. Materials Processing Technology. 209: 2008-2014.

Mahmood Moradi, Majid Ghoreishi. (2011). Influences of laser welding parameters on the geometric profile of Ni-base superalloy Rene 80 weld-bead. Int J Adv Manuf Technol. 55, 205-215.

Mahmoud Moradi, M. Ghoreishi, J. Frostevarg, A. F. H. Kaplan. (2013). An investigation on stability of laser hybrid arc welding. Opt. Laser Eng 51: 481-487.

Mahmoud Moradi, Majid Ghoreishi, Mohammad Javad Torkamany. (2014). Modeling and Optimization of Nd:YAG Laser-TIG Hybrid Welding of Stainless Steel. Journal of lasers in Engineering 27: 211-230.

Mahmoud Moradi, Nahid Salimi, Majid Ghoreishi, Hadi Abdollahi, Mahmoud Shamsborhan, Jan Frostevarg, Torbjörn Ilar, Alexander F. H. Kaplan. (2014). Parameter dependencies in laser hybrid arc welding by design of experiments and by a mass balance. Journal of Laser Applications 24: 022004-9.

Mills K.C. (2002) Recommended values of thermo physical properties for commercial alloys, Wood head Publishing Limited,Abington ,U.K .

Mishra, S. and V. Yadava, (2013). Modeling and optimization of laser beam percussion drilling of thin aluminum sheet. Optics & Laser Technology 48: 461-474.

Mishra, S. and V. Yadava. (2013). Modeling and optimization of laser beam percussion drilling of nickel-based superalloy sheet using Nd: YAG laser. Optics and Lasers in Engineering. 51, 681-695.

Montgomery DC. (2009). Design and analysis of experiments, 7th edn, John Wiley, New York.

Parandoush, P. and A. Hossain. (2014). A review of modeling and simulation of laser beam machining. International Journal of Machine Tools and Manufacture 85: 135-145.

Ram K. Ganesh, Wallace W. Bowley, Robert R. Bellantone, Yukap Hahn. (1994). A Model for Laser Hole Drilling in Metals. Journal of Computational Physics 125: 161-176.

Saeed Assarzadeh, Majid Ghoreishi. (2015). Electro-thermal-based finite element simulation and experimental validation of material removal in static gap singlespark die-sinking electro-discharge machining process. J Engineering Manufacture 20: 1-20.

Solana P, K.P., Dowden JM, Marsden PJ. (1998). An analytical model for the laser drilling of metals with absorption within the vapor. Journal of Physics D: Applied Physics 32: 942-952.

Yi Zhang, Shichun Li, Genyu Chen, Jyoti Mazumder. (2013). Experimental observation and simulation of keyhole dynamics during laser drilling. Optics & Laser Technology 48: 405-414.

Yiming Zhang, Zhonghua Shen, Xiaowu Ni. (2014). Modeling and simulation on long pulse laser drilling processing. International Journal of Heat and Mass Transfer 73: 429-437.

Yinzhou Yan, Lingfei Ji, Yong Bao, Yijian Jiang. (2012). An experimental and numerical study on laser percussion drilling of thick-section alumina. Journal of Materials Processing Technology 212: 1257-1270.